

<https://doi.org/10.1016/j.tca.2020.178785>

## **Development of new graphene/epoxy nanocomposites and study of cure kinetics, thermal and mechanical properties**

Sheikh Rehman<sup>1</sup>, Sufyan Akram<sup>2</sup>, Antonios Kanellopoulos<sup>2</sup>, Ahmed Elmarakbi<sup>3</sup>, Panagiotis G Karagiannidis<sup>1\*</sup>

<sup>1</sup>School of Engineering, Faculty of Technology, University of Sunderland, Sunderland, SR6 0DD, United Kingdom

<sup>2</sup>University of Hertfordshire, School of Engineering and Computer Science, Centre for Engineering Research, College Lane Campus, Hatfield, UK

<sup>3</sup>Department of Mechanical and Construction Engineering, Faculty of Engineering and Environment, Northumbria University, Newcastle, NE18ST, United Kingdom

\*Corresponding author: Panagiotis.Karagiannidis@sunderland.ac.uk

### **Abstract:**

New graphene/polymer nanocomposites were prepared using graphene nanoplatelets (GNPs) and the epoxy system Epilok 60-566/Curamine 32-494. The GNPs were first dispersed into the curamine hardener using bath ultrasonication, followed by the addition of the epoxy resin. The cure kinetics were studied by DSC under non-isothermal and under isothermal conditions. The kinetic parameters of the curing process were determined using the non-isothermal Kissinger and Ozawa-Flynn-Wall models. The degree of curing increased with the addition of GNPs,

while the activation energy decreased by 13.7% for the first reaction and by 6.6% for the second as obtained from Kissinger. An increase in thermal stability by the addition of GNPs was identified in the range of 360-580°C using TGA. In terms of mechanical properties, addition of an optimum amount of 0.5%wt of GNPs in the hardener improved the Young's Modulus by 37%. Nanoindentation measurements showed 9.4% improvement in hardness at 0.7%wt.

## **Keywords**

Graphene/Epoxy Nanocomposites; Differential Scanning Calorimetry; Mechanical Properties; Nanoindentation.

## **1. Introduction**

Polymer matrix nanocomposites are materials which provide a good compromise between properties and weight and have found extensive applications in sectors such as aerospace [1], automotive [2], packaging [3], biomedical [4][5] and many others. By choosing an appropriate combination of polymer matrix and reinforcement agent, a new material can be made that exactly meets the requirements of a certain application.

Inorganic nanomaterials were first used as reinforcement agents in the preparation of polymer nanocomposites, owing to their unique properties and numerous potential applications [6][7][8][9][10][11][12]. Research was mainly focused on layered materials of natural origin, such as sodium montmorillonite (Na-MMT) or synthetic clay, such as layered double hydroxide (LDH) [7][8][9][10][11][13][14]. However, the electrical and thermal conductivities of clay minerals are quite poor [15][16]. In order to overcome these shortcomings, carbon based nanofillers such as carbon black [17], exfoliated graphite (EG) [18], carbon nanotubes (CNT) [19] and carbon nanofibers (CNF) [20] have been used.

Graphene may be preferred over other conventional nanofillers (Na-MMT, LDH, CNT, CNF, EG, etc) owing to its high aspect ratio, large theoretical surface area of 2630 m<sup>2</sup>/g [21], intrinsic strength of 130 GPa [22], a Young Modulus of 1TPa [22], high thermal conductivity (5000 W m<sup>-1</sup>K<sup>-1</sup>) [23], and electrical conductivity (6000 S/cm) [24]. Due to the combination of these exciting properties, graphene is considered one of the best carbon nanofillers available.

The effectiveness of graphene as a nanofiller in various polymeric systems such as epoxy, polystyrene, polyaniline, polyurethane, poly(vinylidene fluoride), Nafion, polycarbonate, poly(ethylene terephthalate) has been reported in a detailed review by Kuilla et al. [25]. Epoxies in particular, are a class of high-performance crosslinked polymers with widespread applications as the main component of adhesives and matrices for structural composites in various industries. Recent developments in graphene/epoxy nanocomposites are well reported in recent reviews [26][27][28][29].

The dispersion of graphene and its derivatives into an epoxy polymer is a crucial step in the synthesis of nanocomposites. A good dispersion of the reinforcing agent ensures a maximum reinforced surface area, which will affect the polymer chains and consequently the properties of the whole matrix [26]. Graphene/epoxy nanocomposites are typically prepared via in-situ curing in which graphene is dispersed within the liquid epoxy oligomer and then the curing agent is added. The high viscosity of epoxy may hinder the uniform dispersion of the nanofiller. For this reason, a solvent is used to facilitate dispersion [26]. Even though the latter method is widely adopted, the necessary solvent removal step consists a drawback, adding manufacturing steps while any solvent residues can deteriorate mechanical properties [30].

The physical properties of epoxy nanocomposites also depend on the curing process, i.e. the reactions of epoxide rings of the resin with the amino groups of the hardener. The understanding of the curing mechanism is essential for the effective design of processing operations and control of the final properties of the cured resin. Differential Scanning

Calorimetry (DSC) has been utilised to monitor the curing process of epoxy resins [31]. DSC can provide excellent determination of onset of cure, heat of cure ( $\Delta H$ ), maximum rate of cure, completion of cure, degree of cure and glass transition temperature ( $T_g$ ). Although there is a number of DSC studies on graphene oxide (GO)/epoxy systems up to date [32][33][34][35], very few studies are reported on the effects of pristine graphene on the cure kinetics of epoxy systems [36]. This is because GO contains significant amount of chemical functional groups (i.e. epoxide, hydroxyl, carboxyl and carbonyl) which promote interfacial interactions with polymer matrices making it more compatible.

The type of graphene used (i.e. geometry and surface chemistry) affects the cure kinetics of the particular resin system in use. Prolongo et al. [36], used GNPs (XG Science M25) with an average thickness of 6 nm and lateral average size 25  $\mu\text{m}$  with diglycidyl ether of bisphenol A (DGEBA) (Araldite F, Ciba) and 4,4'-diaminodiphenylmethane (DDM) (Acros Organics) and found that the curing reaction becomes less exothermic with the presence of GNPs as the nanofiller hindered the epoxy-amine reaction. Qiu et al. studied the effects of GOs into tetrafunctional epoxy resin tetraglycidyl-4,4'-diaminodiphenylmethane (TGDDM) cured with the aromatic diamine 4,4'-diaminodiphenylsulfone (DDS) and found that GO increased the enthalpy of the cure reaction and decreased the activation energy  $E_a$ . Wang et al. observed a maximum reduction of 28.8% in  $E_a$  in the system diglycidyl ether of bisphenol-A (DGEBA)/DDS with addition of GO. On the contrary, increase in  $E_a$  was reported for GO/epoxy nanocomposites by Jouyandeh et al. [37] and Ryu et al. [38] and was attributed to viscosity increase with the addition of the nanofiller hindering the chemical reactions. The disparity in results suggests that nanocomposites are sensitive to the detailed chemistry of the epoxy resin system as well as the functional groups on the surface of the graphene [32]. Despite the improved compatibility of GO with polymer matrices, the preparation of GO requires extensive use of solvents and its properties are inferior over graphene. Hence, new approaches

that use unaltered graphite would have major advantages in terms of properties, cost, and environmental impact [39].

In the present work, new graphene/epoxy polymer nanocomposites were prepared using graphene nanoplatelets (GNPs) and the system epoxy resin Epilok 60-566/Curamine 32-494. The GNPs contained a non-ionic surfactant that aided dispersion in the low viscosity liquid Curamine without the use of solvents. The cure kinetics of the neat epoxy/Curamine system (100/30 w/w=stoichiometric ratio) and the GNPs/epoxy/Curamine system (0.5 or 1.5%wt of GNPs) were studied by Differential Scanning Calorimetry (DSC) under non-isothermal conditions at different heating rates (2, 5, 10 and 20°C/min) and under isothermal conditions (50, 70 and 90°C). The thermal stability of the prepared samples was studied by Thermogravimetric Analysis (TGA) and the Young's Modulus ( $E$ ), Ultimate Tensile Strength ( $UTS$ ), Elongation at break as well as the nanomechanical properties were determined. A reduction in  $E_a$ , was observed and improvements in thermal stability and mechanical properties demonstrating that this is a simple and yet efficient fabrication approach.

## 2. Experimental

### 2.1 Materials

GNPs Elicarb® were provided by Thomas Swan, UK. According to the manufacturer, the GNPs have lateral size between 0.5-5 $\mu$ m, thickness in the range of 10-60nm and contain a non-ionic surfactant. Epilok 60-566 resin was provided by Bitrez, UK. This is a specially formulated liquid mixture of epoxy oligomers with low viscosity (0.7 Pa·s at 25°C) and contains a) oligo(bisphenol-A-co-epichlorhydrin) (CAS number: 25068-38-6 and EC number: 500-033-5) with a number average molecular weight <700 (corresponding to n=0 or 1, Fig.1a) in an amount 30-60%w/w; b) oligo[(phenyl glycidyl ether)-co-formaldehyde] (CAS number: 28064-14-4

and EC number: 608-164-0) with a number average molecular weight about 345 (corresponding to  $n=0$  or 1, Fig.1b) in an amount 10-30%w/w; c) 1,6 hexane diol diglycidyl ether (CAS number: 16096-31-4 and EC number: 240-260-4) (Fig.1c) in an amount 10-30%w/w. Curamine 32-494 curing agent (or hardener) was provided by Bitrez, UK. This is a specially formulated liquid amine-based curing agent that is low in viscosity (0.1 Pa·s at 25°C) and has moderate reactivity. This is 4,4'-methylenebis(cyclohexylamine) (Fig.1d) (CAS number: 1761-71-3 and EC number: 217-168-8) (60-100%) MW=210.36284. The epoxide equivalent weight (EEW) defined as the grams of Epilok 60-566 containing 1gmol of epoxy groups is reported by Bitrez to be minimum=170 g/eq and maximum 190 g/eq (average EEW=180 g/eq). The Curamine 32-494 amine hydrogen equivalent weight (AHEW) was calculated by using the following equation:  $AHEW = \text{molecular weight of the amine} / \text{number of active amine hydrogens}$ . The 4,4'-methylenebis(cyclohexylamine) with a molar mass 210.36284 g/mol contains four active amine hydrogen atoms and acts theoretically as a tetramine. Thus, AHEW of the Curamine is equal to  $210.36284/4 = 52.5921$  g/eq. Since it is assumed that one amine hydrogen reacts with one epoxy group the stoichiometric ratio of Curamine to use with the Epilok is given by the ratio:  $AHEW \times 100 / EEW$  of Epilok or  $52.5921 \times 100 / 180 = 29.22$  phr (phr = parts by weight of Curamine per 100 parts by weight of Epilok). The supplier (Bitrez) of the system Epilok 60-566/ Curamine 32-494 recommends the use of phr=30 and this was used in the present work, which corresponds to the 1:1 stoichiometric ratio of curing agent to the available epoxy groups.

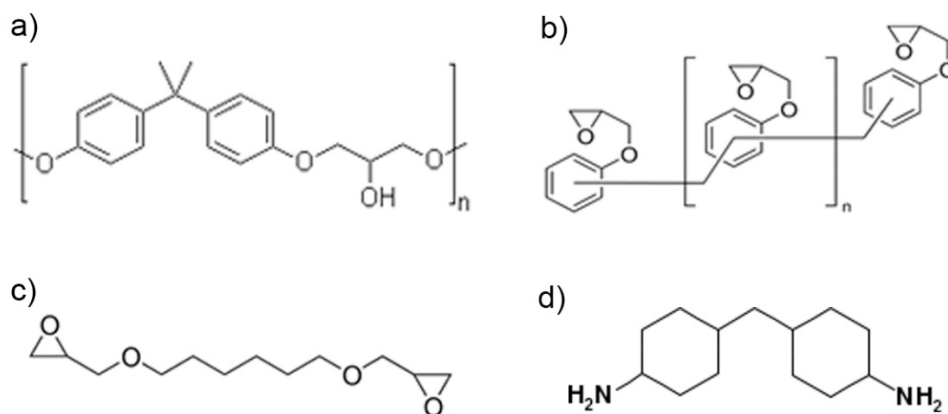


**Figure 1.** (a-c) Chemical structure of epoxy compounds contained in Epilok resin 60-566: a) Oligo(bisphenol-A-co-epichlorohydrin)  $n=0$  or 1, b) Oligo[(phenyl glycidyl ether)-co-formaldehyde]  $n=0$  or 1, c) 1,6 Hexane diol diglycidyl ether. (d) chemical structure of 4,4'-methylenebis(cyclohexylamine) contained in curing agent Curamine 32-494.

## 2.2. Preparation of Nanocomposites

GNPs were first mixed with the Curamine using a bath ultrasonicator (Elmasonic P300) for 20 min. Following ultrasonication, the epoxy resin was added via hand mixing for 3 min at a ratio Epilok:Curamine of 100:30. Samples were prepared for DSC, TGA, mechanical and nanomechanical testing. The methodology followed is summarised in Figure 2.

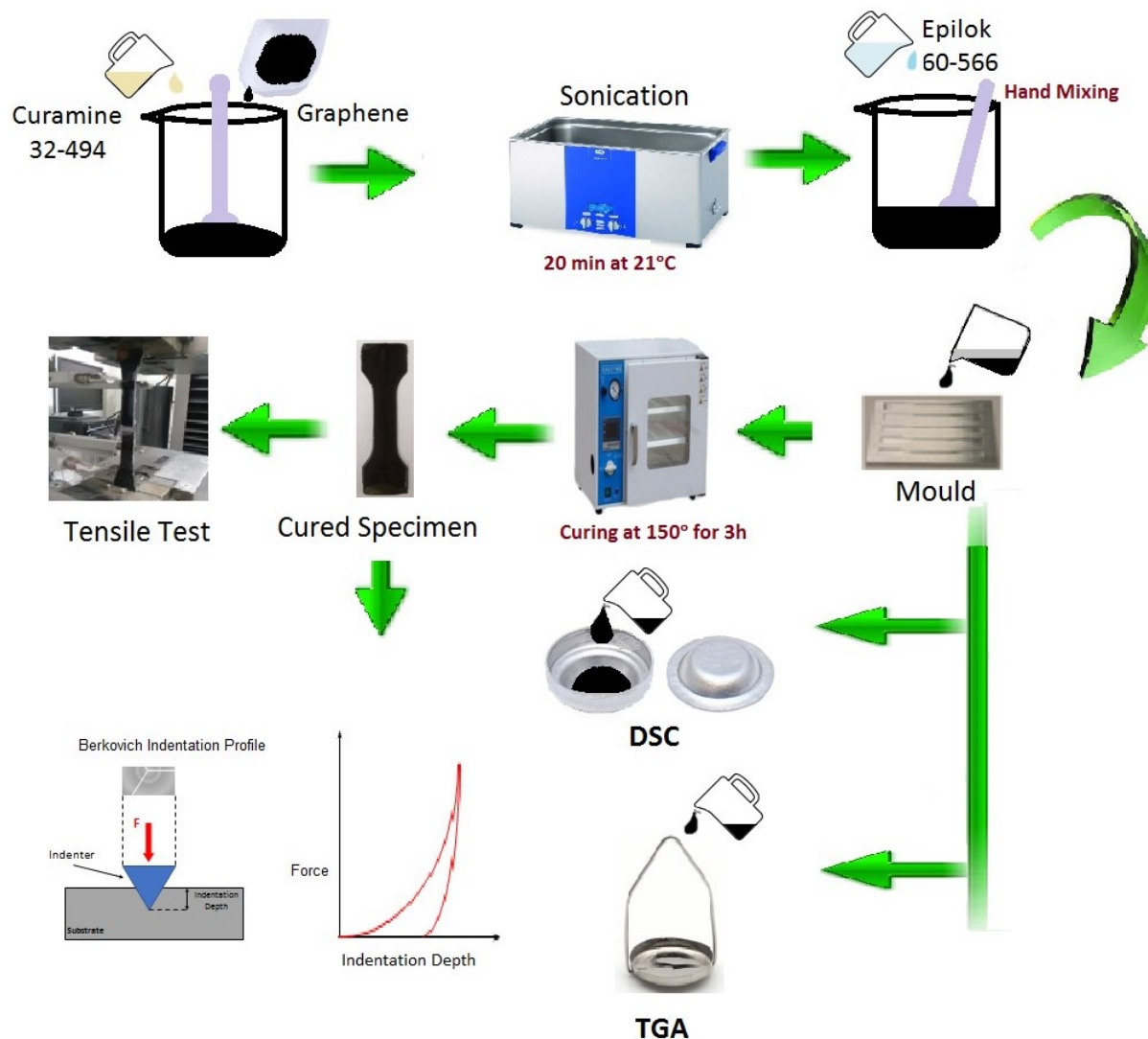


**Figure 2.** Methodology followed for the preparation of GNPs/epoxy nanocomposites and their characterisation by DSC, TGA and mechanical testing.

### 2.3. Curing kinetics by DSC measurements

The DSC study of the neat epoxy system and nanocomposites was carried out using a Differential Scanning Calorimeter DSC Q10 from TA Instruments. The content of GNPs in these samples was 0.5 or 1.5%wt. Samples about 10-15mg were weighted and sealed into

aluminium hermetic DSC pans. The sample pan was then put in the DSC cell previously maintained at room temperature. All DSC runs were carried out under N<sub>2</sub> atmosphere.

Non-isothermal scans were recorded from 20 up to 300°C with four different heating rates 2, 5, 10 or 20°C/min. Isothermal scans were recorded at 50, 70 or 90°C. The DSC cell was quickly heated (50°C/min) to the desired cure temperature and then isothermally held at that temperature for 3h. Following this isothermal scan, the DSC cell was immediately cooled down to room temperature and then heated to 300°C at 10°C/min to obtain the residual heat of curing. This was determined by integrating over the exothermic peak with respect to time. The total heat of curing recorded isothermally ( $\Delta H_{iso}$ ) and the residual heat of curing recorded dynamically ( $\Delta H_{dyn}$ ) were used to determine the degree of curing ( $\alpha$ ) at various isothermal cure temperatures.

#### **2.4 Thermal stability study by TGA**

The thermal stability of the prepared nanocomposites was investigated by thermogravimetric analysis using a TGA55 thermogravimetric analyser by TA Instruments. Measurements were carried out from 20°C to 800°C, at heating rate of 10°C/min under N<sub>2</sub> atmosphere.

#### **2.5 Mechanical characterisation**

Specimens were prepared for tensile tests (~15g/per sample) with GNPs content 0.3, 0.5, 0.7 or 1%wt. After the addition of Epilok resin into graphene/Curamine mixture, mechanical stirring was applied. Aluminum moulds were prepared using a CNC milling machine. The final mixture was poured into the moulds and cured for 3h at 150°C (Fig. 2). Dumbbell-shape specimens were obtained 32mm long and 4mm thick for tensile measurements. Tensile tests

were performed using a universal testing machine Zwick Roell Z010 with a load cell of 10 kN at room temperature with a crosshead speed of 5mm/min. Hardness and  $E$  for all samples were obtained by instrumented indentation. For this purpose, nanoindentation measurements were performed with a Micromaterials NanoTest Vantage platform 3 using a diamond Berkovich indenter. The samples were securely clamped to the nanoindenter and a total of 100 indentations, per sample, were performed applying a maximum load of 10mN with an initial load of 0.1mN, a load time of 10s, a dwell period of 20s and an unloading time of 5s. The indentations were performed using a 10 by 10 grid matrix with 100 $\mu$ m spacing between each indentation. All the tests were performed at room temperature. The inbuilt NanoTest Vantage algorithms were used to calculate hardness.  $E$  was obtained using the following equation:

$$E = \frac{1 - \nu_s^2}{\frac{1}{E_r} - \frac{1 - \nu_i^2}{E_i}} \quad (1)$$

where  $\nu_s$  and  $\nu_i$  are the Poisson's ratios of the sample and the Berkovich indenter,  $E_i$  is the elastic modulus of the indenter and  $E_r$  is the reduced modulus of the sample after indentation. The obtained results were processed with one-way ANOVA parametric analysis using a Tukey's range test.

### 3. Results and discussion

#### 3.1 Curing study by DSC

The main reactions that take place during curing include the epoxide ring at the end of the epoxy resin chains with the primary amino groups (Fig.3a), secondary amino groups (Fig.3b) and etherification of oxirane ring with a pendant hydroxyl group (Fig.3c). These reactions may

take place, either simultaneously or sequentially, depending on the reactivity of reactants and the process temperature.

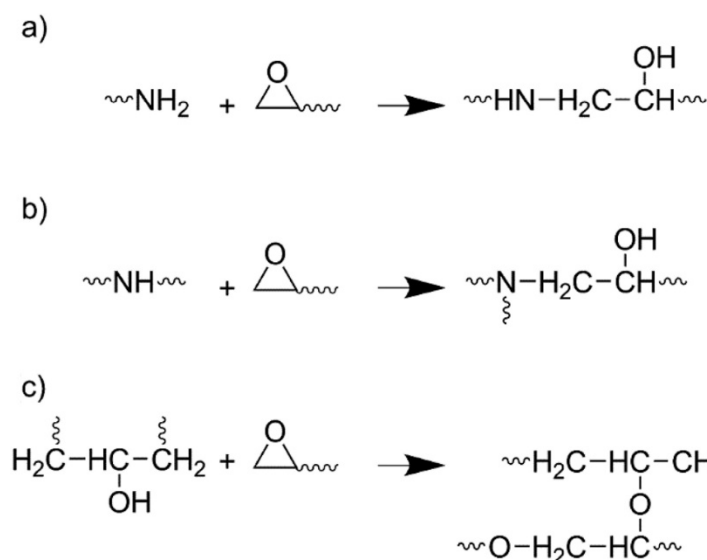


**Figure 3.** Reactions which take place during curing a) epoxide ring at the end of the epoxy resin chains with the primary amino groups b) epoxide ring and secondary amino groups and c) etherification of oxirane ring with a pendant hydroxyl group [40].

Horie et al. [41] observed that the primary amine reaction shows  $E_a$  of 58.2 kJ mol<sup>-1</sup> (13.9 kcal mol<sup>-1</sup>) and the secondary amine reaction 56.1 kJ mol<sup>-1</sup> (13.4 kcal mol<sup>-1</sup>). For 1:1 stoichiometry as in our case, or when amine is present in excess, reaction (c) (Fig. 3) is generally insignificant with respect to reactions (a) and (b). In most systems, the primary and secondary amines have similar reactivities and one DSC cure exotherm is observed. In few cases, e.g. with hindered amines [42], the reactivity of secondary amine may be significantly lower, resulting in separate exotherms; one for the reaction of primary amine with epoxy, and the other for secondary amine with epoxy. Such cases are observed in hindered amines in which the nitrogen atom of the amine molecule is partially shielded by neighbouring groups so that larger molecules cannot

easily approach and react with the nitrogen. Etherification reaction (Fig.3c) is usually much slower than the amine-epoxy reactions and only becomes significant in epoxy-rich systems above 150°C when the primary amine is sufficiently depleted [43]; two cure exotherms are typically observed in epoxy-rich systems.

Curing of epoxy resins is a highly exothermic process, hence reaction kinetics were monitored by recording the amount of heat released with time (rate of heat flow in Watts=J/s) by DSC under non-isothermal and isothermal conditions. The basic assumption underlying the application of DSC is that the measured rate of heat flow ( $dH/dt$ ) is proportional to the reaction rate  $da/dt$ :

$$\frac{da}{dt} = \frac{1}{\Delta H_{total}} \left( \frac{dH}{dt} \right) \quad (2)$$

where  $\Delta H_{total}$  is the exothermic heat expressed as heat per mole of reacting groups ( $\text{kJ mol}^{-1}$ ). In the ideal case,  $\Delta H_{total}$  is the total heat liberated when an uncured resin is taken to complete cure and this value is independent of temperature for a particular resin system. The degree of curing  $\alpha$  at any time  $t$  is given by

$$\alpha(t) = \frac{\Delta H(t)}{\Delta H_{total}} \quad (3)$$

where  $\Delta H(t)$  is the heat generated up to time  $t$ . The ultimate degree of conversion is defined as

$$\alpha_{ult} = \frac{\Delta H_{ult}}{\Delta H_{total}} \quad (4)$$

For several amine-epoxy systems and model reactions,  $\Delta H_{total}$  has been measured and found to be reasonably constant and equal to  $25.6 \pm 1$  kcal mol<sup>-1</sup> of epoxide ( $107 \pm 4$  kJ mol<sup>-1</sup> of epoxide); this value may be used as a standard value for analyzing amine-epoxide systems [44], [31]. However, it was found from simultaneous DSC and FTIR measurements conflicting results for  $\Delta H_{total}$ , that is  $83 \pm 2$ ,  $131 \pm 9$ , and  $65 \pm 6$  kJ mol<sup>-1</sup> for primary amine (Fig.3a), secondary amine (Fig.3b) and hydroxyl (Fig.3c) reactions with epoxide respectively; note that the average for the primary plus secondary amine reactions is 107 kJ mol<sup>-1</sup> [45]. It is worth noting that values of  $25.5 \pm 1.5$  kcal mol<sup>-1</sup> of epoxide are typically measured in epoxy systems with excess amine (e.g. up to 20%), but lower values are often observed for 1:1 stoichiometric mixture suggesting that 100% conversion may be difficult to achieve in stoichiometric systems [46] [47] [48].

### 3.1.1. Non-isothermal scanning method

The non-isothermal DSC curves for the neat epoxy resin system and the composite with 0.5 or 1.5%wt of GNPs at different heating rates (2, 5, 10 and 20°C/min) were recorded. Characteristic curves illustrating the change of heat flow with temperature for the neat epoxy resin and the nanocomposite with 1.5%wt GNPs are shown in Figure 4.

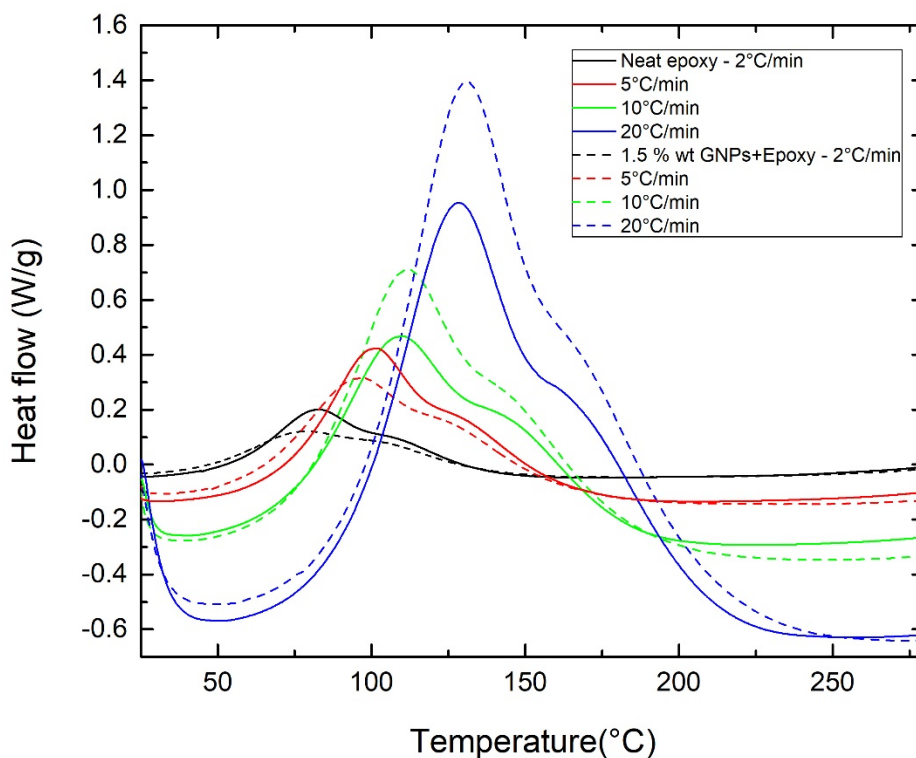


**Figure 4.** Dynamic scans with different heating rates 2-20°C/min for neat epoxy and with 1.5%wt GNPs.

All DSC curves showed a broad peak and a shoulder at higher temperature, which further will be referred to as peak-1 and peak-2. An analogous result was reported for the non-isothermal curing study by DSC of the commercial epoxy resin Epikote 828 based on diglycidyl ether of bisphenol A cured by isophorone diamine (Fig.5). One peak was first observed which was attributed to the reaction of epoxy group with the aliphatic group  $-CH_2NH_2$  and a shoulder attributed to the alicyclic group [49].

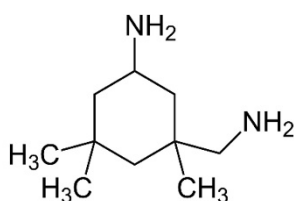


**Figure 5.** Chemical structure of isophorone diamine a cycloaliphatic diamine [49].

A non-isothermal curing study by DSC of two systems Epikote resin 816LV/Epikure F205 and Epikote resin 240/Epikure F205 (at stoichiometric ratio) was also reported in literature [50]. The epoxy resin is based on a diglycidyl ether of bisphenol A and the curing agent is based on isophorone diamine. In both cases, first a peak and then a shoulder was observed in all scans carried out at different scanning rates. Study of isothermal (30, 50 and 70°C) curing kinetics of these systems by Fourier Transform Infrared Spectroscopy (FTIR) showed that the reaction of hydroxyl groups with the epoxy groups does not seem to take place.

According to the literature data reported above, in our case the first peak observed in DSC (Fig.4) must correspond to the reaction of primary amino group with the epoxy (Fig.3a) and the second to the reaction of secondary amino group with the epoxy group (Fig.3b). It is worth to note that 4,4'-methylenebis(cyclohexylamine) contained in Curamine 32-494 is a hindered amine with the two amino groups  $-NH_2$  connected with alicyclic groups (Fig.1d); so the secondary amino group  $-NH-$  derived from reaction (a) (Fig.3) shows much lower reactivity than the primary amino group  $-NH_2$ . Hence, the reaction (b) (Fig.3) gives the shoulder at higher temperature (Fig.4). Since we used 1:1 stoichiometric mixture the reaction between the hydroxyl group and epoxy (Fig. 3c) does not take place.

The initial curing temperature ( $T_{init}$ ), final ( $T_{final}$ ) and the peak temperatures, ( $T_{peak-1}$ ) and ( $T_{peak-2}$ ) shift to a higher values with increasing heating rate  $\phi$  (Table 1). No significant peak shift is observed with the addition of graphene. From a practical standpoint it may be desirable to define processing parameters such as  $T_{init}$  and  $T_{final}$ ; for example, a practical definition of  $T_{final}$  could be the minimum cure temperature at which total ( $\alpha=1$ ) or final ( $\alpha=\alpha_{final}$ ) conversion takes place in a reasonable time.

**Table 1.** Characteristic temperatures of curing process obtained under non-isothermal conditions with different heating rates.

GNPs (%wt)	$\phi$ (°C/min)	$T_{init}$ (°C)	$T_{final}$ (°C)	$T_{final}-T_{int}$ (°C)	$T_{peak-1}$ (°C)	$T_{peak-2}$ (°C)
<b>0</b>	2	18.5	261.1	243.7	81.5	108.3
	5	20.9	273.0	252.0	99.8	130.8
	10	26.6	291.3	264.7	108.8	147.1
	20	35.8	298.4	262.6	129.9	171.6
<b>0.5</b>	2	17.9	278.5	260.6	82.8	108.1
	5	20.3	274.4	254.0	90.4	121.7
	10	21.3	285.2	263.9	112.2	149.0
	20	30.5	292.5	262.0	123.7	168.2
<b>1.5</b>	2	15.4	270.3	254.9	76.5	104.9
	5	25.8	284.6	258.8	94.5	127.8
	10	23.3	286.8	263.5	110.5	147.7
	20	36.6	291.3	254.7	129.9	171.4

The ultimate heat of curing  $\Delta H1_{ult}$  (kJ/g) and  $\Delta H2_{ult}$  (kJ/g) were determined by integration of the peak-1 and peak-2 correspondingly. Taking into account that we have used a ratio of 100g epoxy resin to 30g of amine, 1g of the mixture contains 0.796g of epoxy resin, and since the EEW of epoxy resin used is average 180g/eq (=the grams of Epilok 60-566 containing 1gmol of epoxy groups), the values of  $\Delta H1_{ult}$  (kJ/mol) and  $\Delta H2_{ult}$  (kJ/mol) were calculated by  $\Delta H1_{ult}$  (kJ/g)<sub>epoxy</sub> x 180 and  $\Delta H2_{ult}$  (kJ/g)<sub>epoxy</sub> x 180 correspondingly. The two experimental peaks were deconvoluted using OriginPro and a Lorentzian function with adjusted  $R^2 = 0.998$ . All values obtained for  $\Delta H$  and  $\alpha$  are shown in Table 2.

**Table 2.** Exothermic heat of curing ( $\Delta H$ ) and degree of curing ( $\alpha$ ) obtained under non-isothermal conditions with different heating rates.

GNPs (%wt)	$\varphi$ (°C/min)	$\Delta H_{1ult}$ (J/g)*	$\Delta H_{2ult}$ (kJ/mol)**	$\Delta H_{2ult}$ (J/g)*	$\Delta H_{2ult}$ (kJ/mol)**	$\alpha_1$ (%)	$\alpha_2$ (%)	$\alpha$ (%)
0	2	222.02	51.96	91.04	21.30	63	16	79
	5	244.31	57.18	108.66	25.43	69	19	88
	10	213.38	49.94	91.28	21.36	60	16	76
	20	241.44	56.51	88.33	20.67	68	16	84
0.5	2	210.91	49.36	103.08	24.12	59	18	77
	5	211.64	49.53	107.32	25.12	60	19	79
	10	272.91	63.88	101.89	23.84	77	18	95
	20	269.19	63.00	111.26	26.04	76	20	96
1.5	2	155.76	36.45	95.48	22.34	44	17	61
	5	227.01	53.13	108.32	25.35	64	19	83
	10	282.5	66.12	111.72	26.15	80	19	99
	20	293.25	68.64	96.06	22.48	83	17	100

\*  $\Delta H_{1ult}$  (J/g) refers to 1gr of epoxy determined from the experimental value divided by 0.769.

\*\* $\Delta H_{ult}$  (kJ/mol) calculated from  $\Delta H_{ult}$  (kJ/g) x 180 (=EEW of Epilok 60-566).

The degree of curing was calculated from equation 4, where for peak-1 the value of  $\Delta H_{total} = 83$  kJ/mol was used and for peak-2 (shoulder) the value of  $\Delta H_{total} = 131$  kJ/mol [45]. The total degree of curing is  $\alpha = \alpha_1 + \alpha_2$  [51][52]. The lower  $\alpha$  values obtained for the loading 0.5 and 1.5 %wt GNPs at low heating rates 2 and 5°C/min than the neat epoxy/amine system can be attributed to the steric hindrance of GNPs. The main reason is the low interaction between the GNPs and the matrix, generating a very weak interface [53]. On the contrary, the higher  $\alpha$

obtained for the loading 0.5 and 1.5 %wt GNPs at high heating rates 10 and 20°C/ min, than the  $\alpha$  of neat epoxy/amine system can be attributed to high thermal conductivity of GNPs (Table 2).

One of the most frequently used model-free methods which estimate  $E_a$  and the pre-exponential factor ( $A$ ) in physical or chemical processes from data obtained at several non-isothermal tests conducted at constant heating rates (constant during each test, different among tests) is the Kissinger method [54] and is identical to the ASTM Method E 698-79 [55]. Kissinger derived a useful expression that relate  $E_a$  and  $A$  for  $n^{\text{th}}$ -order reactions to  $\varphi$  and peak temperature  $T_p$  [49]

$$A = \frac{\varphi E e^{\frac{E_a}{RT_p}}}{RT_p^2 [n(1 - a_p)^{n-1}]} \quad (5)$$

Kissinger argued that  $n(1 - a_p)^{n-1} \approx 1$  and is independent of the heating rate; obviously, by definition, this is true for a first-order reaction [56] and showed this quantity to be constant and only 2-4% greater than unity for an  $n^{\text{th}}$ -order cure reaction. Kissinger in his study of reactions of any order  $n$  observed that the peak shape of a reaction is independent of heating rate and the values of the kinetic constants and depends only on the reaction order  $n$ ; to quantitatively describe the peak shape a “shape index” ( $S$ ) was proposed defined as the absolute value of the ratio of the slopes of tangents to the curve at the inflection points ( $S=a_1/a_2$ , Fig. 6a). The shape index  $S$  is then a function only of the reaction order  $n$ :

$$S = 0.63n^2 \Rightarrow n = 1.26 S^{1/2} \quad (6)$$

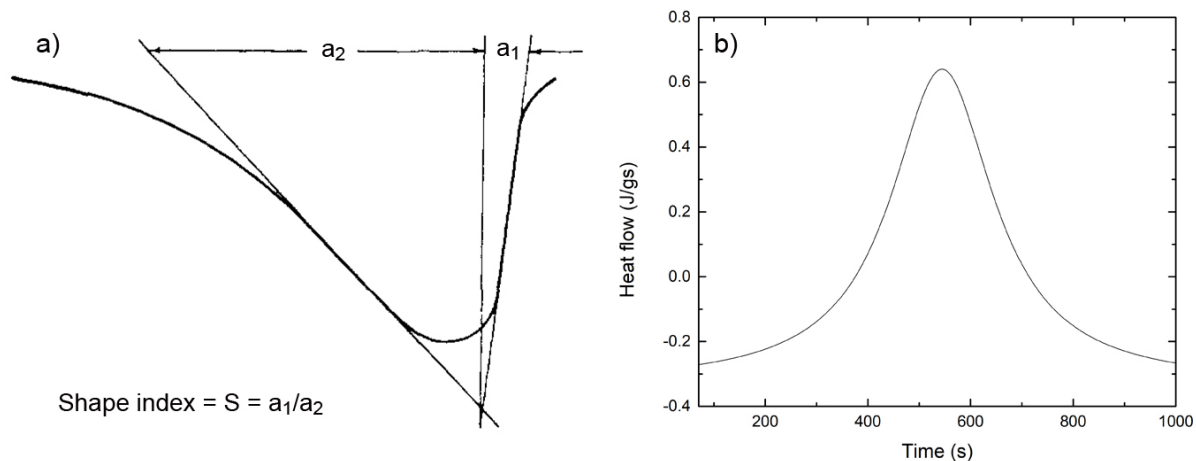


**Figure 6.** a) Determination of shape index  $S$  of DSC curves [54], b) deconvoluted peak-1.

Thus equation (6) leads to the result  $n=1.26$ . So, equation (5) can be written as:

$$A = \frac{\varphi E e^{\frac{E_a}{RT_p}}}{RT_p^2} \quad (7)$$

And taking the logarithm of eq. (7) we take:

$$\ln\left(\frac{\varphi}{T_p^2}\right) = \ln\left(\frac{AR}{E_a}\right) - \frac{E_a}{RT_p} \quad (8)$$

Where  $R$  is the universal gas constant ( $8.314 \times 10^{-3}$  kJ/mol·K). By plotting  $\ln(\varphi/T_p^2)$  versus  $1/T_p$ , the values of  $E_a$  and the  $A$  can be estimated from the slope of the linear fit and the y-intercept correspondingly. However, it must be noted that the Kissinger method is associated with the fact that the determination of accurate  $E_a$  values requires  $a_p$  (eq. 5) to be independent of  $\varphi$ . Otherwise the plot of  $\ln(\varphi/T_p^2)$  versus  $1/T_p$  would deviate systematically from a straight line. It is reported that for other models  $\alpha$  at  $T_p$  may vary significantly with  $\varphi$  [51]. A variation of  $\alpha$  at  $T_p$  with  $\varphi$  can be detected on visual inspection as a change in the peak shape with  $\varphi$  [51]. The peak shape of the studied epoxy/amine system in this work was found to be symmetrical and

practically unchanged for all heating rates. The shape index (S) of peaks (representative peak-1 is shown in Fig. 6b) was calculated as  $S = a_1 + a_2$ , which corresponds based on eq. 6 to  $n = 1.26$ . From the plot of  $\ln(\phi/T_p^2)$  versus  $1/T_p$  shown in Fig. 7, the value of activation energy  $E_{a1}$  was determined for the neat epoxy to be  $51.09 \pm 4.74$  kJ/mol and  $A_1 = 3489.9$  s<sup>-1</sup> and  $E_{a2} = 44.64 \pm 2.29$  kJ/mol and  $A_2 = 101.26$  s<sup>-1</sup> for peak-2. The values of  $E_{a1}$  and  $E_{a2}$  for primary and secondary amino groups of our system obtained by Kissinger method are lower than those reported by Horie [41]. Addition of 1.5%wt GNPs dropped values to  $E_{a1} = 44.10 \pm 1.48$  kJ/mol and  $A_1 = 357.69$  s<sup>-1</sup> and  $E_{a2} = 41.68 \pm 0.90$  kJ/mol and  $A_2 = 41.35$  s<sup>-1</sup>.

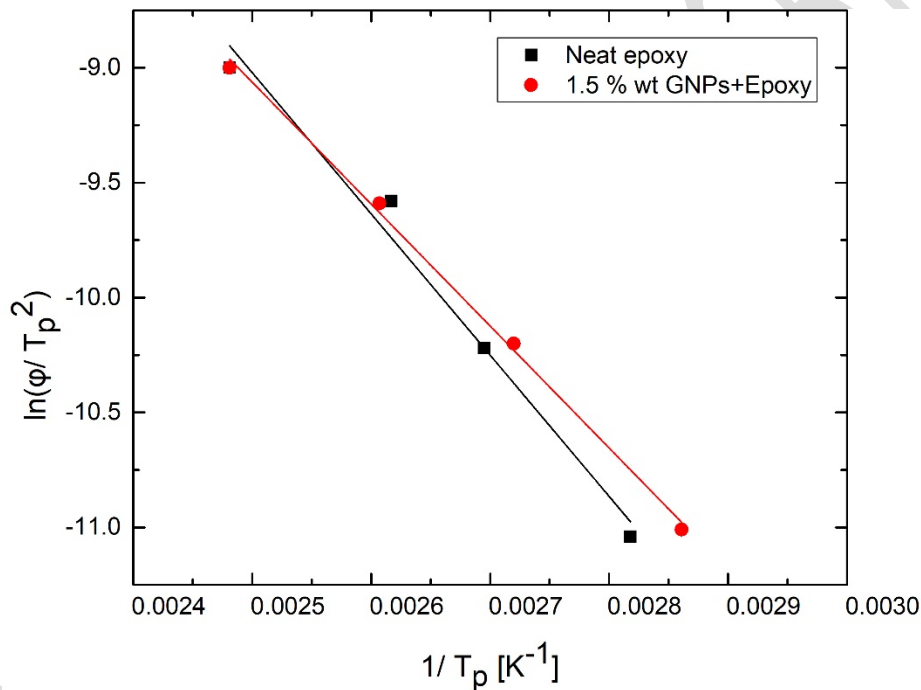


**Figure 7.** Kissinger's plot to determine  $E_a$  from the slope of the linear fit and factor  $A$  from the y-intercept for peak-1.

$E_a$  is the minimum energy requirement that must be met for a chemical reaction to occur; the factor  $A$  is an empirical relationship between temperature and rate constant  $k$  and depends on the quantity of molecules or groups in the reaction and their orientation. Both  $E_a$  and  $A$  connect with the reaction rate constant  $k$  with an Arrhenius-type expression:

$$k = Ae \left( -\frac{E_a}{RT} \right) \quad (9)$$

where  $k$  is the rate constant (for order one, the rate constant has units of  $s^{-1}$ ). From  $E_a$  and  $A$  data based on the Arrhenius law, the rate constants  $k_1$  and  $k_2$  and ratio  $k_1/k_2$  at different temperature can be derived. The results obtained are shown in Table 3. These results show that the values of  $E_a$  and  $A$  and  $k_1/k_2$  are lower for the secondary imino -NH- group. As it can be seen, as the temperature increases both reactions proceed simultaneously; both constants  $k_1$  and  $k_2$  increase with temperature but the ratio  $k_1/k_2$  remains constant. This shows that the participation ratio of the primary amino group and the secondary amino groups to the reactions (Fig.3a) and (Fig.3.b) correspondingly is constant and the structure of the prepared polymer matrix does not depend on the curing temperature.

Table 3 shows that the loading of 1.5 %wt GNPs led to a significant decrease of  $k_1/k_2$ , which was due mainly to the significant decrease of  $k_1$ . Two opposite effects have to be considered in order to explain in the epoxy curing in presence of graphene, the steric hinderance of GNPs that impedes the mobility of the reactants decreasing the curing reaction rate and the high thermal conductivity of GNPs which can explain the accelerating effect for high temperatures [36]. The significant decrease of  $k_1$ , an order of magnitude, and of  $k_2$  and so  $k_1/k_2$  with the presence of 1.5 %wt GNPs can be attributed to the steric hindrance of GNPs.

**Table 3.** Rate constants  $k_1$  and  $k_2$  and ratio  $k_1/k_2$  at different temperatures.

T (K)	Neat epoxy			1.5%wt GNPs + epoxy		
	$k_1$ ( $s^{-1}$ )	$k_2$ ( $s^{-1}$ )	$k_1/k_2$	$k_1$ ( $s^{-1}$ )	$k_2$ ( $s^{-1}$ )	$k_1/k_2$
298.15	3418.70	99.45	34.38	351.38	40.66	8.64
308.15	3420.99	99.51	34.38	351.58	40.68	8.64

318.15	3423.13	99.56	34.38	351.77	40.70	8.64
328.15	3425.15	99.61	34.39	351.95	40.72	8.64
338.15	3427.05	99.66	34.39	352.12	40.74	8.64
348.15	3428.84	99.71	34.39	352.28	40.75	8.64
358.15	3430.53	99.75	34.39	352.43	40.77	8.64
368.15	3432.13	99.79	34.39	352.57	40.79	8.64
378.15	3433.64	99.83	34.39	352.70	40.80	8.64
388.15	3435.08	99.86	34.40	352.83	40.81	8.64
398.15	3436.45	99.90	34.40	352.95	40.83	8.64

It is worth noting that although the Kissinger method produces unambiguous Arrhenius parameters, it yields a single averaged pair of these parameters for the overall cure process in a manner similar to the model-fitting methods, which can be used however for comparative studies e.g. the effect of GNPs on the epoxy resin curing. The resulting average values do not reflect changes in the reaction mechanism and kinetics with the curing temperature and  $\alpha$ . However, the process of epoxy curing is known to involve multiple steps that are likely to have different  $E_a$  values. Then the contributions of these steps to the overall cure rate measured by DSC should vary with both temperature and  $\alpha$ . The amine-epoxy reactions (Fig. 3.a-b) may be uncatalysed (n order) or catalysed by probable impurities (e.g. water, alcohols, phenols, acids) initially present in the reaction system (n order) or by the hydroxyl groups (OH) generated by the epoxy-amine reaction (autocatalysis) (m order) [57][58][59][60]. During curing the reaction system undergoes gelation (liquid-to-rubber) and vitrification (rubber-to glass) transitions. Intensive crosslinking occurring in the region between the above transitions reduces molecular mobility and the cure changes from a kinetic to a diffusion regime [61]. In such cases where changes in the curing mechanism are associated with changes in the activation energy the model-free isoconversional methods can be used to observe how the activation energy changes throughout the entire

reaction. One of the model-free isoconversional methods, the Ozawa-Flynn-Wall analysis provide a simple relationship between  $\alpha$  dependent  $E_\alpha$ ,  $\varphi$  and isoconversion temperature ( $T_i$ ) [62]:

$$\log\varphi = -\frac{0.4567E_\alpha}{RT_i} + A' \quad (10)$$

for each relative degree of curing ( $\alpha_r$ ),  $A'$  is a constant that can be defined as:

$$A' = \log\left(\frac{AE_\alpha}{g(\alpha)R}\right) - 2.315 \quad (11)$$

where  $g(\alpha)$  is a conversion dependent function. In order to determine the corresponding  $E_\alpha$  and  $A$  at each relative  $\alpha$ , a plot first was drawn of relative degree of cure ( $\alpha_r$ ) vs curing temperature ( $T$ ) at each  $\varphi$ , as shown in Fig. 8.a,b and Fig. 8.c,d. for peak-1 and peak-2 correspondingly.

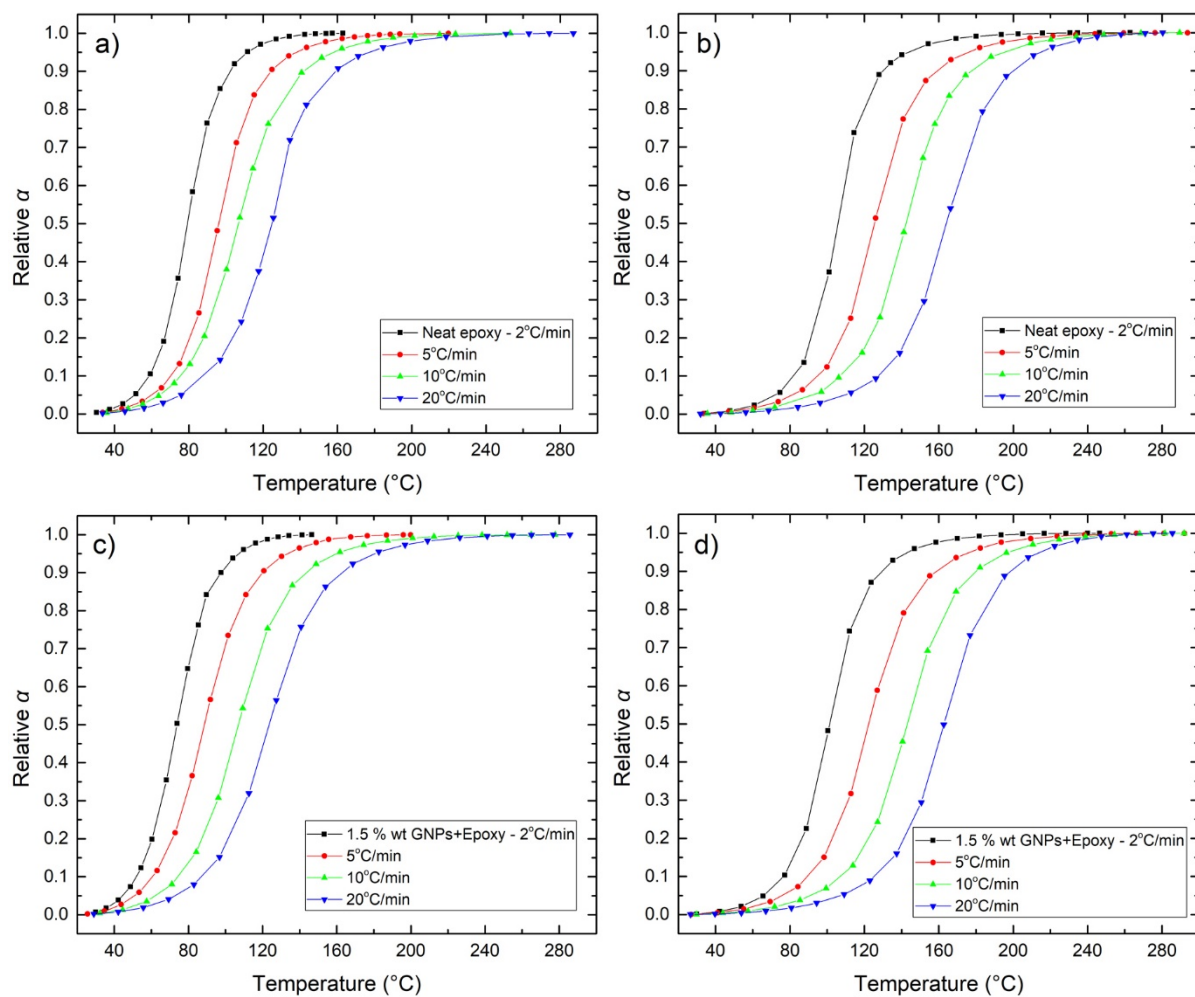


**Figure 8.** Conversion  $\alpha$  as a function of temperature at different heating rates for a) neat epoxy peak-1, b) neat epoxy peak-2, c) 1.5 %wt GNP/epoxy peak-1 and d) 1.5 %wt GNP/epoxy peak-2.

Then a plot of  $\log \phi$  vs  $T_i$  was drawn at each  $\alpha_r$  as shown in Fig. 9.a,b. The resulting slope is proportional to  $E_\alpha$  and the intercept is proportional to  $A'$ .

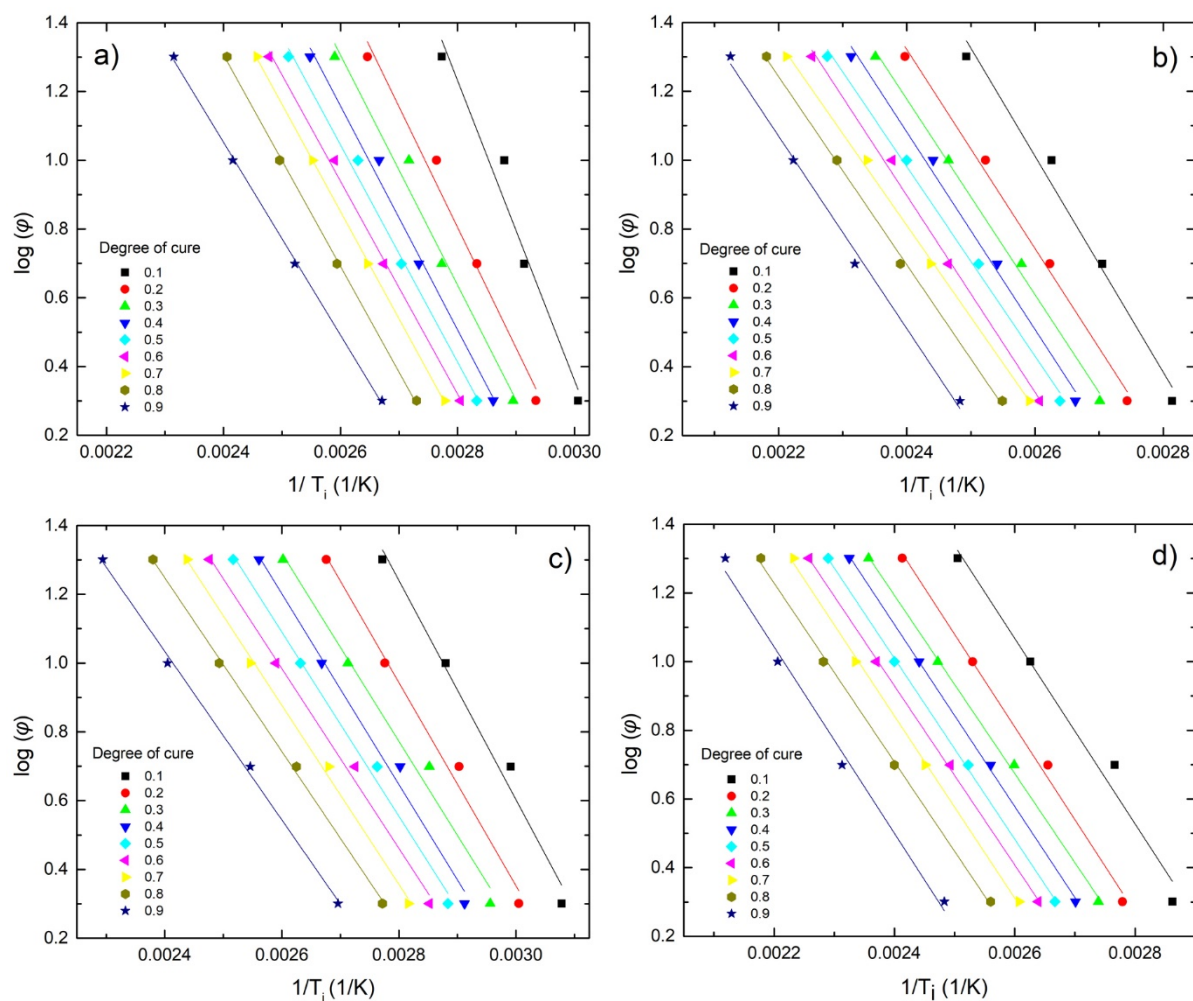


**Figure 9.** Isoconversional plots for the logarithmic heating rate versus the reciprocal of the absolute temperature for a) neat epoxy peak-1, b) neat epoxy peak-2, c) 1.5 %wt GNP/epoxy peak-1 and d) 1.5 %wt GNP/epoxy peak-2.

In Fig. 10.a,b the  $E_{\alpha}$  was plotted with  $\alpha$ , for neat epoxy resin and GNPs/epoxy composite with 1.5%wt GNPs for peak-1 and peak-2. The high effective value of  $E_{\alpha}$  at the very beginning of curing at  $\alpha=1$  corresponds to the non-catalysed reaction epoxy-amine. Since the hydroxyl groups formed during the curing facilitate the ring opening (autocatalysis) it is reasonable to expect then a rapid decrease in  $E_{\alpha}$ . From Fig.10a-b it observed that  $E_{\alpha 1}$  decreases from 79.5 to 51 kJ/mol for the neat epoxy and  $E_{\alpha 2}$  from 57.1 to 50.9 kJ/mol. The nanocomposite contained

1.5wt% showed a decrease in  $E_{a1}$  from 58.2 to 44.6 kJ/mol and  $E_{a2}$  is about 48 kJ/mol. The minimum values are close to the ones calculated by the Kissinger method.

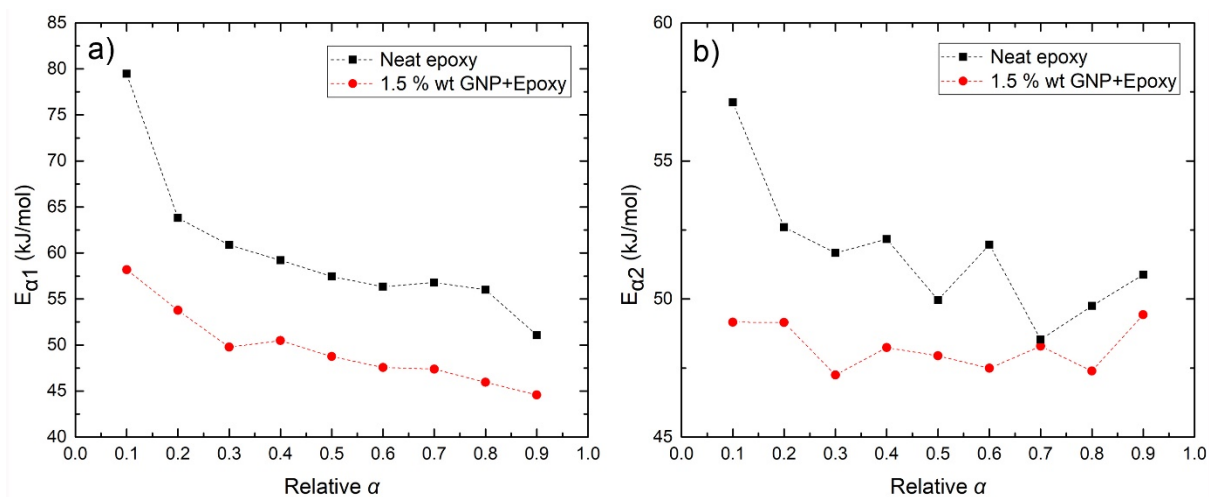


**Figure 10.** Ozawa–Flynn–Wall’s activation energy ( $E_{\alpha}$ ) as a function of relative degree of cure  $\alpha$  for a) peak-1 and b) peak-2.

### 3.1.2. Isothermal scanning method

Isothermal DSC curves at 50, 70 and 90°C are presented in Figure 11. A single exothermic peak was observed for each isothermal run which corresponds to maximum curing rate. Figure 11 shows that the reaction rate at  $t=0$  is zero which indicate that the epoxy-amine reaction is non-catalysed (n-order) and then as the OH groups forms facilitate the ring opening (m-order) (autocatalysis) [61]. The peak value decreases in intensity and shifts to longer times at lower temperature. The total curing enthalpy  $\Delta H_{iso}$  at a certain temperature and time was determined.

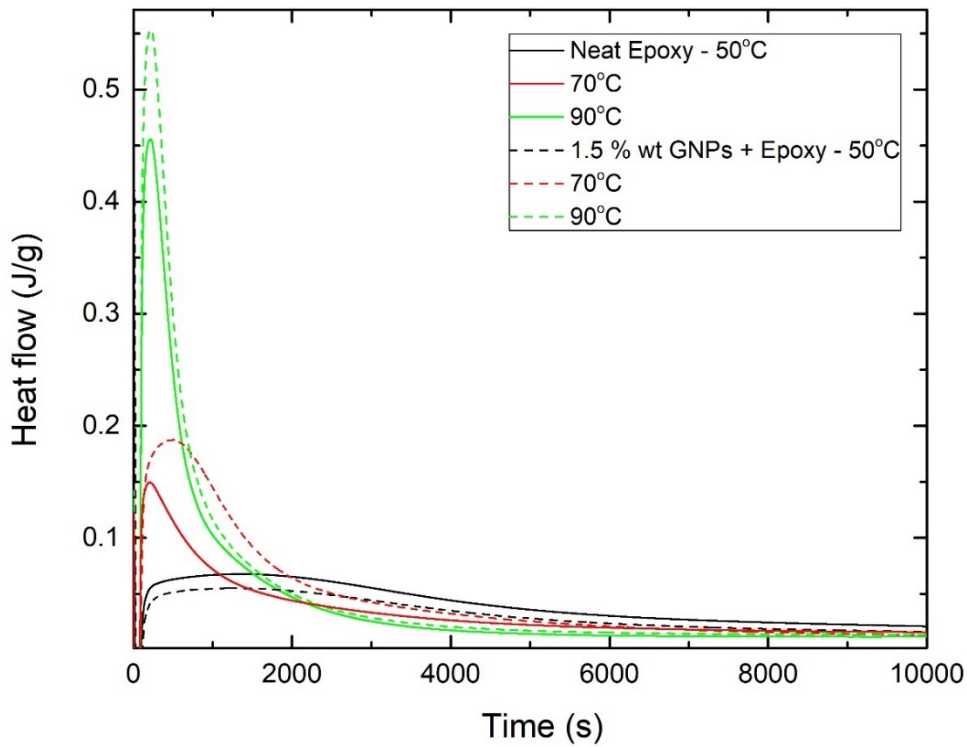


**Figure 11.** Isothermal DSC thermograms for neat epoxy and nanocomposites containing 1.5%wt GNPs at different temperatures.

Following the isothermal scans, the samples immediately cooled at room temperature and then heated to 300°C at 10°C/min. The curves obtained are shown in Figure 12. From the data shown in Table 4, a relative degree of conversion  $\alpha_1$  can be calculated as:

$$\alpha_1 = \frac{\Delta H_{iso}}{\Delta H_{iso} + \Delta H_{dyn}} \quad (12)$$

The degree of conversion was also calculated from equation 4, using  $\Delta H_{tot}$  of 107 kJ/mol being the average enthalpy for primary and secondary reactions [45].

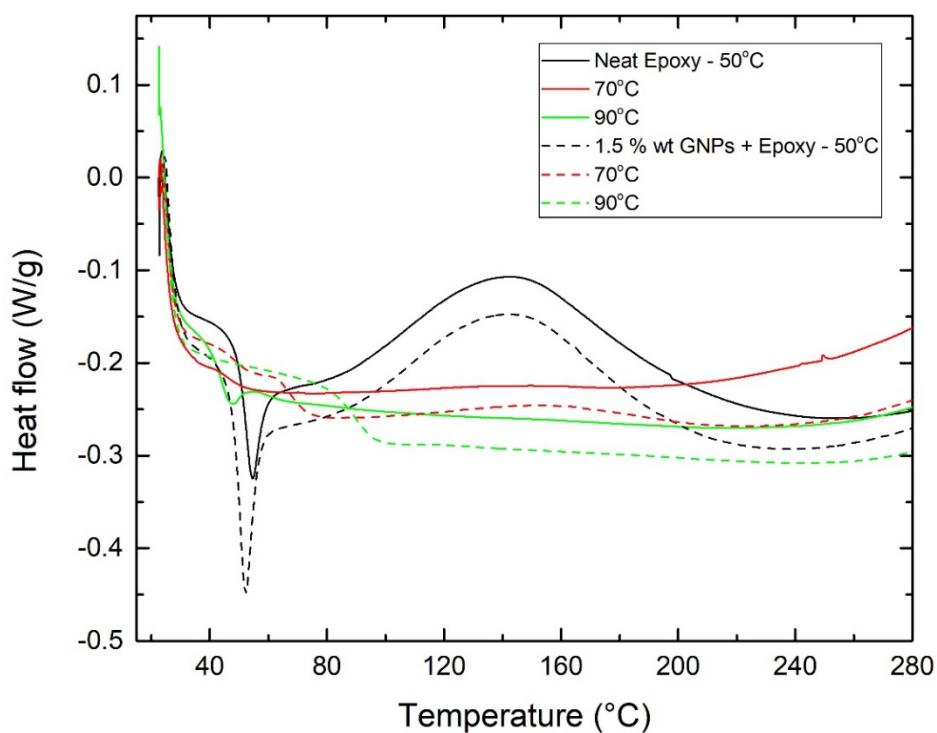


**Figure 12.** Subsequent non-isothermal DSC scans at constant heating rate of the partially cured samples derived from the isothermal scans.

Table 4 summarises the obtained heat of curing values from the isothermal scans  $\Delta H_{iso}$ , the dynamic  $\Delta H_{dyn}$ ,  $\alpha_1$  and  $\alpha_2$  and  $T_g$ . The isothermally cured neat epoxy and nanocomposite at 90°C didn't show any residual enthalpy in the subsequent dynamic scan. As expected,  $\alpha_1$ ,  $\alpha_2$  and  $T_g$  increase with the increase of curing temperature. It can be seen that  $\alpha$  increases with the addition of GNPs.

**Table 4.** Exothermic heat of curing during the isothermal scans ( $\Delta H_{iso}$ ), during subsequent dynamic scans ( $\Delta H_{dyn}$ ), degree of curing ( $\alpha$ ) and glass transition temperature ( $T_g$ ).

GNPs (%wt)	T (°C)	$\Delta H_{iso}^*$ (kJ/mol)	$\Delta H_{dyn}$ (kJ/mol)	$\alpha_1$ (%)	$\alpha_2$ (%)	$T_g$ (°C)
0	50	49.51	14.47	77.4	46.3	54.5
	70	52.17	1.57	97.1	48.7	72.1
	90	60.56	0	100	56.5	84.5
1.5	50	37.15	14.14	72.4	34.7	52.0
	70	72.82	1.14	98.4	68.0	78.5
	90	80.87	0	100	75.6	88.5

\* $\Delta H_{ult}$  (kJ/mol) calculated from  $\Delta H_{ult}$  (kJ/g) x 180 (=EEW of Epilok 60-566) where  $\Delta H_{ult}$  (kJ/g) refers to 1gr of epoxy determined from the experimental value divided by 0.769.

It is observed that the values of  $\alpha_1$  and  $\alpha_2$  for 1.5 %wt GNPs in epoxy system were lower than those of neat epoxy from the isothermal DSC measurements under 50°C, which is different from the trends under 70°C and 90°C. At low temperature 50°C the steric hindrance of GNPs interfered with the mobility of the reactive species. The higher temperatures 70°C and 90°C prompted the mobility of the reacting species, increased the local density of the reacting species and prompted the curing reaction. On the other hand, the high thermal conductivity of the GNPs further weakened the retarding effect of the steric hindrance from the added GNPs. An analogous behaviour is reported in [63].

### 3.2. Thermogravimetric analysis

Figure 13 presents TGA curves of the epoxy and the nanocomposites containing 1.5%wt GNPs. The initial decomposition temperature which corresponds to 5% weight loss [33] was found to decrease from 339°C for the neat epoxy to 330°C for the nanocomposite. This could result from the early decomposition of the interfacial epoxy chains, the cure of which was partially

inhibited by the inclusion of GNPs [33]. The dominant weight loss occurs above 350°C due to the thermal decomposition of epoxy resin. The temperature of the maximum rate of degradation decrease from 392.3°C of the neat epoxy resin to 378.6°C in the case of the nanocomposite. The TGA curve of the GNP/epoxy nanocomposite was shifted in the range of 360-580°C towards higher temperature compared to that of pure epoxy increasing the thermal stability of the cured epoxy composites. The % weight residue at 500°C is 7.85% for the neat and 22.45% for the nanocomposite.

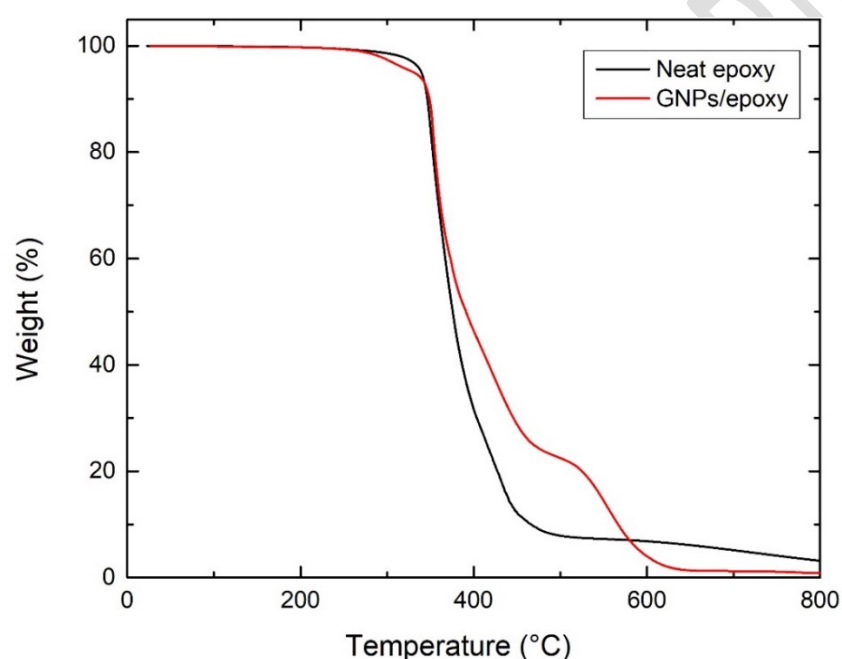


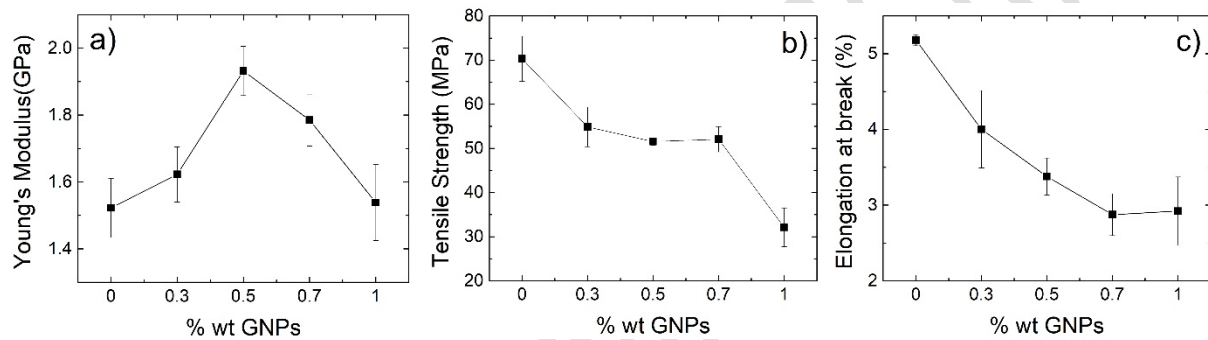
**Figure 13.** TGA spectra obtained from neat epoxy and cured nanocomposites containing 1.5%wt GNPs.

### 3.3 Mechanical Properties

#### 3.3.1 Tensile

Figure 14 presents the mechanical properties of the prepared nanocomposites as a function of the %wt GNPs. The addition of graphene caused an increase in  $E$  at low filler content which

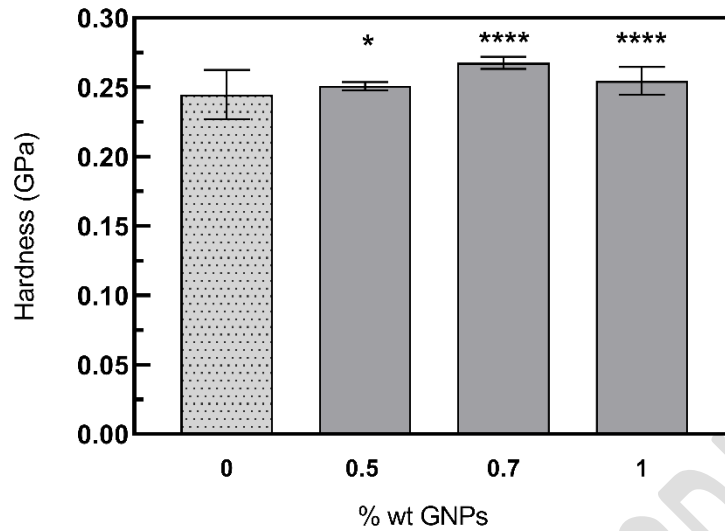
was peaked at 0.5%wt and then decrease. The maximum enhancement in  $E$  was 37% (1.98 GPa compared to 1.58GPa of the neat epoxy). Addition of graphene flakes into the polymer matrix caused a reduction in UTS from 70.3MPa for the neat epoxy to 32.1MPa for 1%wt GNPs. The mechanical properties in graphene/epoxy nanocomposites are strongly dependent on the sample preparation conditions (dispersion steps, use of solvent etc); hence a direct comparison with other reports is difficult. However, similar trend in  $E$  and  $UTS$  was observed by I. Zaman et al. [64] and Poutrel et al [65] which was attributed to poor interfacial bonding between the epoxy and graphene.



**Figure 14.** Mechanical properties of cured nanocomposites; a) Young's Modulus, b) Tensile Strength and c) Elongation at break.

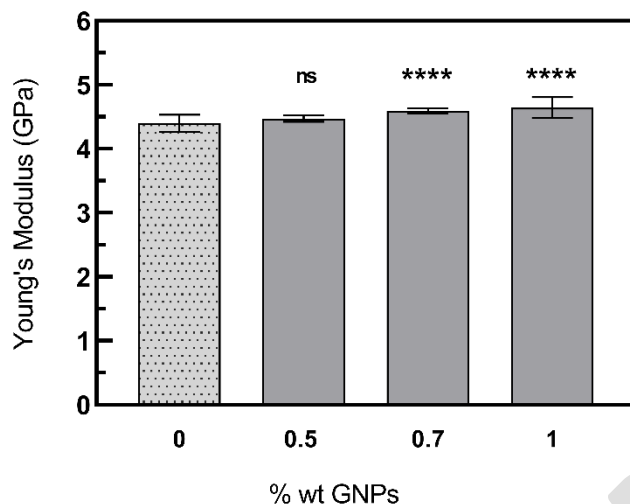
### 3.3.2 Nanoindentation

Figure 15 shows the hardness are determined by the nanoindentation test. Analysis of the data showed that there are statistical differences between the samples with the samples enriched with 0.7% GNPs showing a 9.4% improvement over the neat epoxy.



**Figure 15.** Instrumented indentation hardness values for all samples. Values are means  $\pm$ SD. P-values calculated by Tukey's range test: \*p-value < 0.05; \*\*\*\*p < 0.0001.

Figure 16 shows  $E$  as determined by the nanoindentation. Analysis of the data showed that there are statistical differences between the control sample and the 0.7% and 1%wt nanocomposites but not for the 0.5% wt. The improvement for the latter is in the range of 1.7% and increases to 4.5% and 5.6% for nanocomposites enriched with 0.7% and 1% GNPs. The  $E$  values determined by nanoindentation, although follow the same trend, are higher than those obtained by macroscopic tensile tests. This is in agreement with other reports and is likely due to pile up of material around the contact impression [66][67].



**Figure 16.** Instrumented indentation elastic modulus values for all samples. Values are means  $\pm$ SD. P-values calculated by Tukey's range test: ns = no statistical significance; \*\*p-value < 0.01; \*\*\*\*p < 0.0001.

### 3.5 Acknowledgments

The authors would like to thank Bitrez Ltd and Thomas Swan & Co. Ltd. for providing the epoxy resin and graphene materials respectively.

### 4. Conclusions

In summary, we studied the cure kinetics, thermal stability and mechanical properties of GNP/Epilok 60-566 prepared via a solvent-free facile approach by dispersing GNPs in the curing agent Curamine 32-494. DSC analysis showed that the degree of cure was increased with the addition of GNPs at high heating rates (10-20°C/min). It was found that the addition of 1.5%wt GNPs catalysed the curing reactions;  $E_a$  was found to decrease by 13.7% and by 6.6% for the reactions of the primary and secondary amino groups with the epoxy group

respectively. The GNPs also improved the thermal stability of the epoxy system in the range of 360-580°C. An increase in Young's Modulus was observed in all nanocomposites containing GNPs from 0.3 to 0.7%wt with maximum enhancement of 37% at 0.5%wt. Nanoindentation measurements showed 9.4% improvement in hardness at 0.7%wt.

### Data Availability

The raw/processed data required to reproduce these findings cannot be shared at this time as the data also forms part of an ongoing study.

### References

- [1] J. Njuguna and K. Pieliowski, "Polymer Nanocomposites for Aerospace Applications: Properties," *Advanced Engineering Materials*. 2003, doi: 10.1002/adem.200310101.
- [2] A. K. Naskar, J. K. Keum, and R. G. Boeman, "Polymer matrix nanocomposites for automotive structural components," *Nature Nanotechnology*. 2016, doi: 10.1038/nnano.2016.262.
- [3] A. Kausar, "A review of high performance polymer nanocomposites for packaging applications in electronics and food industries," *Journal of Plastic Film and Sheeting*. 2020, doi: 10.1177/8756087919849459.
- [4] W. Qi, X. Zhang, and H. Wang, "Self-assembled polymer nanocomposites for biomedical application," *Current Opinion in Colloid and Interface Science*. 2018, doi: 10.1016/j.cocis.2018.01.003.
- [5] Y. Lu, M. C. Biswas, Z. Guo, J. W. Jeon, and E. K. Wujcik, "Recent developments in bio-monitoring via advanced polymer nanocomposite-based wearable strain sensors,"

- Biosensors and Bioelectronics*. 2019, doi: 10.1016/j.bios.2018.08.037.
- [6] D. Y. Godovsky, "Device applications of polymer-nanocomposites," *Advances in Polymer Science*. 2000, doi: 10.1007/3-540-46414-x\_4.
- [7] M. Alexandre and P. Dubois, "Polymer-layered silicate nanocomposites: Preparation, properties and uses of a new class of materials," *Mater. Sci. Eng. R Reports*, 2000, doi: 10.1016/S0927-796X(00)00012-7.
- [8] S. Sinha Ray and M. Okamoto, "Polymer/layered silicate nanocomposites: A review from preparation to processing," *Progress in Polymer Science (Oxford)*. 2003, doi: 10.1016/j.progpolymsci.2003.08.002.
- [9] Z. Zhang *et al.*, "Partial delamination of the organo-montmorillonite with surfactant containing hydroxyl groups in maleated poly(propylene carbonate)," *Polymer (Guildf)*., 2006, doi: 10.1016/j.polymer.2006.09.041.
- [10] P. Li, N. H. Kim, S. Bhadra, and J. H. Lee, "Electroresponsive property of novel poly(acrylate- acryloyloxyethyl trimethyl ammonium chloride)/clay nanocomposite hydrogels," in *Advanced Materials Research*, 2009, doi: 10.4028/www.scientific.net/AMR.79-82.2263.
- [11] F. Leroux and J. Besse, "Polymer interleaved layered double hydroxide: A new emerging class of nanocomposites," *Chemistry of Materials*. 2001, doi: 10.1021/cm0110268.
- [12] T. Kuila, S. K. Srivastava, A. K. Bhowmick, and A. K. Saxena, "Thermoplastic polyolefin based polymer - blend-layered double hydroxide nanocomposites," *Compos. Sci. Technol.*, 2008, doi: 10.1016/j.compscitech.2008.08.003.
- [13] E. P. Giannelis, R. Krishnamoorti, and E. Manias, "Polymer-silicate nanocomposites:

- Model systems for confined polymers and polymer brushes,” *Adv. Polym. Sci.*, 1999, doi: 10.1007/3-540-69711-x\_3.
- [14] S. Pavlidou and C. D. Papaspyrides, “A review on polymer-layered silicate nanocomposites,” *Progress in Polymer Science (Oxford)*. 2008, doi: 10.1016/j.progpolymsci.2008.07.008.
- [15] N. J. García and J. C. Bazán, “Electrical conductivity of montmorillonite as a function of relative humidity: La-montmorillonite,” *Clay Miner.*, 2009, doi: 10.1180/claymin.2009.044.1.81.
- [16] Y. Z. Bao, L. F. Cong, Z. M. Huang, and Z. X. Weng, “Preparation and proton conductivity of poly(vinylidene fluoride)/layered double hydroxide nanocomposite gel electrolytes,” *J. Mater. Sci.*, 2008, doi: 10.1007/s10853-007-2100-1.
- [17] Q. Li, O. K. Park, and J. H. Lee, “Positive temperature coefficient behavior of HDPE/EVA blends filled with carbon black,” in *Advanced Materials Research*, 2009, doi: 10.4028/www.scientific.net/AMR.79-82.2267.
- [18] B. Debelak and K. Lafdi, “Use of exfoliated graphite filler to enhance polymer physical properties,” *Carbon N. Y.*, 2007, doi: 10.1016/j.carbon.2007.05.010.
- [19] Z. Spitalsky, D. Tasis, K. Papagelis, and C. Galiotis, “Carbon nanotube-polymer composites: Chemistry, processing, mechanical and electrical properties,” *Progress in Polymer Science (Oxford)*. 2010, doi: 10.1016/j.progpolymsci.2009.09.003.
- [20] V. Khanna and B. R. Bakshi, “Carbon nanofiber polymer composites: Evaluation of life cycle energy use,” *Environ. Sci. Technol.*, 2009, doi: 10.1021/es802101x.
- [21] Y. Zhu *et al.*, “Graphene and graphene oxide: Synthesis, properties, and applications,” *Adv. Mater.*, 2010, doi: 10.1002/adma.201001068.

- [22] C. Lee, X. Wei, J. W. Kysar, and J. Hone, "Measurement of the elastic properties and intrinsic strength of monolayer graphene," *Science (80-. )*, 2008, doi: 10.1126/science.1157996.
- [23] A. A. Balandin *et al.*, "Superior thermal conductivity of single-layer graphene," *Nano Lett.*, 2008, doi: 10.1021/nl0731872.
- [24] X. Du, I. Skachko, A. Barker, and E. Y. Andrei, "Approaching ballistic transport in suspended graphene," *Nat. Nanotechnol.*, 2008, doi: 10.1038/nnano.2008.199.
- [25] T. Kuilla, S. Bhadra, D. Yao, N. H. Kim, S. Bose, and J. H. Lee, "Recent advances in graphene based polymer composites," *Prog. Polym. Sci.*, 2010, doi: 10.1016/j.progpolymsci.2010.07.005.
- [26] J. Wei, T. Vo, and F. Inam, "Epoxy/graphene nanocomposites - processing and properties: a review," *RSC Adv.*, 2015, doi: 10.1039/c5ra13897c.
- [27] R. Shah, A. Kausar, B. Muhammad, and S. Shah, "Progression from Graphene and Graphene Oxide to High Performance Polymer-Based Nanocomposite: A Review," *Polym. - Plast. Technol. Eng.*, 2015, doi: 10.1080/03602559.2014.955202.
- [28] R. Atif, I. Shyha, and F. Inam, "Mechanical, thermal, and electrical properties of graphene-epoxy nanocomposites-A review," *Polymers*, vol. 8, no. 8. 2016, doi: 10.3390/polym8080281.
- [29] A. Kausar, Z. Anwar, and B. Muhammad, "Recent Developments in Epoxy/Graphite, Epoxy/Graphene, and Epoxy/Graphene Nanoplatelet Composites: A Comparative Review," *Polymer - Plastics Technology and Engineering*. 2016, doi: 10.1080/03602559.2016.1163589.
- [30] R. Atif, I. Shyha, and F. Inam, "The degradation of mechanical properties due to stress

- concentration caused by retained acetone in epoxy nanocomposites,” *RSC Adv.*, 2016, doi: 10.1039/c6ra00739b.
- [31] R. B. Prime, “Thermosets,” in *Thermal Characterization of Polymeric Materials*, Second., E. A. Turi, Ed. Academic Press, San Diego, 1997, pp. 1380–1744.
- [32] D. G. D. Galpaya *et al.*, “The effect of graphene oxide and its oxidized debris on the cure chemistry and interphase structure of epoxy nanocomposites,” *Polymer (Guildf)*., 2015, doi: 10.1016/j.polymer.2015.06.054.
- [33] X. Wang, J. Jin, M. Song, and Y. Lin, “Effect of graphene oxide sheet size on the curing kinetics and thermal stability of epoxy resins,” *Mater. Res. Express*, 2016, doi: 10.1088/2053-1591/3/10/105303.
- [34] S. L. Qiu *et al.*, “Effects of graphene oxides on the cure behaviors of a tetrafunctional epoxy resin,” *Express Polym. Lett.*, 2011, doi: 10.3144/expresspolymlett.2011.79.
- [35] C. Monteserín, M. Blanco, E. Aranzabe, A. Aranzabe, and J. L. Vilas, “Effects of graphene oxide and chemically reduced graphene oxide on the curing kinetics of epoxy amine composites,” *J. Appl. Polym. Sci.*, 2017, doi: 10.1002/app.44803.
- [36] M. G. Prolongo, C. Salom, C. Arribas, M. Sánchez-Cabezudo, R. M. Masegosa, and S. G. Prolongo, “Influence of graphene nanoplatelets on curing and mechanical properties of graphene/epoxy nanocomposites,” *J. Therm. Anal. Calorim.*, 2016, doi: 10.1007/s10973-015-5162-3.
- [37] M. Jouyandeh *et al.*, “Cure kinetics of epoxy/graphene oxide (GO) nanocomposites: Effect of starch functionalization of GO nanosheets,” *Prog. Org. Coatings*, 2019, doi: 10.1016/j.porgcoat.2019.105217.
- [38] S. H. Ryu, J. H. Sin, and A. M. Shanmugaraj, “Study on the effect of hexamethylene

- diamine functionalized graphene oxide on the curing kinetics of epoxy nanocomposites,” *Eur. Polym. J.*, 2014, doi: 10.1016/j.eurpolymj.2013.12.014.
- [39] S. J. Woltornist, J. M. Y. Carrillo, T. O. Xu, A. V. Dobrynin, and D. H. Adamson, “Polymer/pristine graphene based composites: From emulsions to strong, electrically conducting foams,” *Macromolecules*, 2015, doi: 10.1021/ma5024236.
- [40] R. Ramsdale-Capper and J. P. Foreman, “Internal antiplasticisation in highly crosslinked amine cured multifunctional epoxy resins,” *Polymer (Guildf.)*, 2018, doi: 10.1016/j.polymer.2018.05.048.
- [41] K. Horie, H. Hiura, M. Sawada, I. Mita, and H. Kambe, “Calorimetric investigation of polymerization reactions. III. Curing reaction of epoxides with amines,” *J. Polym. Sci. Part A-1 Polym. Chem.*, 1970, doi: 10.1002/pol.1970.150080605.
- [42] J. V. Duffy, E. Hui, and B. Hartmann, “Reaction kinetics for hindered amine/epoxides by DSC,” *J. Appl. Polym. Sci.*, 1987, doi: 10.1002/app.1987.070330828.
- [43] C. C. Riccardi and R. J. J. Williams, “A kinetic scheme for an amine-epoxy reaction with simultaneous etherification,” *J. Appl. Polym. Sci.*, 1986, doi: 10.1002/app.1986.070320208.
- [44] D. Verchère, H. Sautereau, J. P. Pascault, C. C. Riccardi, S. M. Moschiar, and R. J. J. Williams, “Buildup of epoxyaliphatic amine networks. Kinetics, vitrification, and gelation,” *Macromolecules*, 1990, doi: 10.1021/ma00205a006.
- [45] C. J. de Bakker, N. A. St John, and G. A. George, “Simultaneous differential scanning calorimetry and near-infra-red analysis of the curing of tetraglycidyl-diaminodiphenylmethane with diaminodiphenylsulphone,” *Polymer (Guildf.)*, 1993, doi: 10.1016/0032-3861(93)90353-C.

- [46] C. C. Riccardi, H. E. Adabbo, and R. J. J. Williams, "Curing reaction of epoxy resins with diamines," *J. Appl. Polym. Sci.*, 1984, doi: 10.1002/app.1984.070290805.
- [47] S. L. Simon and J. K. Gillham, "Reaction kinetics and TTT cure diagrams for off-stoichiometric ratios of a high-Tg epoxy/amine system," *J. Appl. Polym. Sci.*, 1992, doi: 10.1002/app.1992.070460714.
- [48] S. L. Simon and J. K. Gillham, "Thermosetting cure diagrams: Calculation and application," *J. Appl. Polym. Sci.*, 1994, doi: 10.1002/app.1994.070530601.
- [49] L. Núñez, F. Fraga López, L. Fraga Grueiro, and J. A. Rodríguez Añón, "Activation energies and rate constants for an epoxy/cure agent reaction: Variation in peak exotherm temperature," *J. Therm. Anal.*, 1996, doi: 10.1007/BF01981809.
- [50] D. S. Achilias, M. M. Karabela, E. A. Varkopoulou, and I. D. Sideridou, "Cure kinetics study of two epoxy systems with Fourier Transform Infrared Spectroscopy (FTIR) and Differential Scanning Calorimetry (DSC)," *J. Macromol. Sci. Part A Pure Appl. Chem.*, 2012, doi: 10.1080/10601325.2012.696995.
- [51] S. Vyazovkin, A. K. Burnham, J. M. Criado, L. A. Pérez-Maqueda, C. Popescu, and N. Sbirrazzuoli, "ICTAC Kinetics Committee recommendations for performing kinetic computations on thermal analysis data," *Thermochim. Acta*, vol. 520, no. 1, pp. 1–19, 2011, doi: <https://doi.org/10.1016/j.tca.2011.03.034>.
- [52] C. Jubsilp, K. Punson, T. Takeichi, and S. Rimdusit, "Curing kinetics of Benzoxazine–epoxy copolymer investigated by non-isothermal differential scanning calorimetry," *Polym. Degrad. Stab.*, vol. 95, no. 6, pp. 918–924, 2010, doi: <https://doi.org/10.1016/j.polymdegradstab.2010.03.029>.
- [53] S. G. Prolongo, R. Moriche, A. Jiménez-Suárez, M. Sánchez, and A. Ureña,

- “Advantages and disadvantages of the addition of graphene nanoplatelets to epoxy resins,” *Eur. Polym. J.*, vol. 61, pp. 206–214, 2014, doi: <https://doi.org/10.1016/j.eurpolymj.2014.09.022>.
- [54] H. E. Kissinger, “Reaction Kinetics in Differential Thermal Analysis,” *Anal. Chem.*, 1957, doi: 10.1021/ac60131a045.
- [55] D. K. Hadad, “Physical and Chemical Characterization of Epoxy Resins,” in *Epoxy Resins Chemistry and Technology*, Second., C. A. May, Ed. Taylor & Francis Inc , CRC Press Inc, 1988.
- [56] R. B. Prime, “Differential scanning calorimetry of the epoxy cure reaction,” *Polym. Eng. Sci.*, 1973, doi: 10.1002/pen.760130508.
- [57] P. I. Karkanis and I. K. Partridge, “Cure modeling and monitoring of epoxy/amine resin systems. I. Cure kinetics modeling,” *J. Appl. Polym. Sci.*, vol. 77, no. 7, pp. 1419–1431, Aug. 2000, doi: 10.1002/1097-4628(20000815)77:7<1419::AID-APP3>3.0.CO;2-N.
- [58] B. A. Rozenberg, “Kinetics, thermodynamics and mechanism of reactions of epoxy oligomers with amines BT - Epoxy Resins and Composites II,” 1986, pp. 113–165.
- [59] S. Swier, G. Van Assche, W. Vuchelen, and B. Van Mele, “Role of Complex Formation in the Polymerization Kinetics of Modified Epoxy–Amine Systems,” *Macromolecules*, vol. 38, no. 6, pp. 2281–2288, Mar. 2005, doi: 10.1021/ma047796x.
- [60] H. J. Flammersheim, “Kinetics and mechanism of the epoxide–amine polyaddition | Presented at the Twelfth Ulm-Freiberg Conference, Freiberg, Germany, 19–21 March 1997,” *Thermochim. Acta*, vol. 310, no. 1, pp. 153–159, 1998, doi: [https://doi.org/10.1016/S0040-6031\(97\)00225-6](https://doi.org/10.1016/S0040-6031(97)00225-6).

- [61] S. Vyazovkin and N. Sbirrazzuoli, "Mechanism and kinetics of epoxy-amine cure studied by differential scanning calorimetry," *Macromolecules*, 1996, doi: 10.1021/ma951162w.
- [62] R. Hardis, J. L. P. Jessop, F. E. Peters, and M. R. Kessler, "Cure kinetics characterization and monitoring of an epoxy resin using DSC, Raman spectroscopy, and DEA," *Compos. Part A Appl. Sci. Manuf.*, 2013, doi: 10.1016/j.compositesa.2013.01.021.
- [63] Y. Fu and W.-H. Zhong, "Cure kinetics behavior of a functionalized graphitic nanofiber modified epoxy resin," *Thermochim. Acta*, vol. 516, no. 1, pp. 58–63, 2011, doi: <https://doi.org/10.1016/j.tca.2011.01.016>.
- [64] I. Zaman *et al.*, "Epoxy/graphene platelets nanocomposites with two levels of interface strength," *Polymer (Guildf)*, 2011, doi: 10.1016/j.polymer.2011.02.003.
- [65] Q. A. Poutrel, Z. Wang, D. Wang, C. Soutis, and M. Gresil, "Effect of pre and Post-Dispersion on Electro-Thermo-Mechanical Properties of a Graphene Enhanced Epoxy," *Appl. Compos. Mater.*, 2017, doi: 10.1007/s10443-016-9541-0.
- [66] J. A. King, D. R. Klimek, I. Miskioglu, and G. M. Odegard, "Mechanical properties of graphene nanoplatelet/epoxy composites," *J. Appl. Polym. Sci.*, 2013, doi: 10.1002/app.38645.
- [67] D. Tranchida, S. Piccarolo, J. Loos, and A. Alexeev, "Mechanical characterization of polymers on a nanometer scale through nanoindentation. A study on pile-up and viscoelasticity," *Macromolecules*, 2007, doi: 10.1021/ma062140k.